applied optics

Compact polarization beam splitter assisted by subwavelength grating in triple-waveguide directional coupler

Tianye Huang,[1,2] Yuan Xie,[1] Yiheng Wu,[1] Zhuo Cheng,[1,*] Shuwen Zeng,[3] and Perry Shum Ping[4]

[1]Mechanical Engineering and Electronic Information, China University of Geosciences (Wuhan), Wuhan 430070, China
[2]Hubei Key Laboratory of Inland Shipping Technology, Wuhan, China
[3]XLIM Research Institute, University of Limoges, Limoges CEDEX, France
[4]Center of Fiber Technology, School of Electrical and Electronic Engineering, Nanyang Technological University, Singapore, Singapore
*Corresponding author: chengzhuo@cug.edu.cn

Received 28 November 2018; revised 21 February 2019; accepted 22 February 2019; posted 25 February 2019 (Doc. ID 352998); published 15 March 2019

A polarization beam splitter (PBS) is one of the key components for manipulating different polarization states in the areas of optical interconnection and communication. In this paper, a PBS with two coupling regions using a subwavelength grating (SWG) waveguide as a bridge is proposed and investigated on a 340-nm silicon-on-insulator platform. The PBS is designed with a triple-waveguide directional coupler consisting of two identical silicon waveguides and an SWG waveguide sandwiched between them. The tailorable dispersion relation of the SWG waveguide offers a flexible design freedom. With the optimized grating period and duty ratio, the input TE mode will experience efficient coupling between the silicon waveguide and the SWG waveguide, while the TM mode can directly pass through without influence. The results show that with a device length of 6.5 μm, the extinction ratios and insertion losses of the two modes are higher than 27 dB and lower than 0.3 dB at a wavelength of 1550 nm, respectively.

https://doi.org/10.1364/AO.58.002264

1. INTRODUCTION

A polarization beam splitter (PBS) is a significant part of photonic integrated circuits [1], which can solve the polarization-sensitive operation caused by birefringence in a photonic waveguide [2]. Many designs for PBSs have been demonstrated to date, such as the Mach–Zehnder interferometer [3], multimode interference (MMI) coupler [4,5], directional couplers (DCs) [6–8], slot waveguides [9,10], and photonic crystal structures [11,12]. Among these structures, the DC is a good choice for its simple design, high efficiency, and good performance. Kim *et al.* demonstrated an integrated PBS based on a DC with high polarization extinction ratio (ER) of ∼40 dB, but the coupling length is 29.4 μm [13]. Feng *et al.* proposed a PBS based on an asymmetric slot structure with ∼14 dB, ∼25 dB (TE and TM mode) ER and ∼18 μm coupling length [14]. Note that such DCs composed by pure silicon waveguides are generally long in size, which can limit high-density on-chip integration. There are also PBSs with small footprint based on bent DC [15,16] or hybrid plasmonic waveguides [17–19]. However, the bent DC requires a precise manufacturing process since a lot of structural parameters are needed to be determined. While generally speaking, the utilization of metal will bring higher loss and fabrication difficulties. Therefore, a PBS formed by pure silicon with short length and simple structure is highly desired [20].

A grating is a structure in which different refractive index materials alternate periodically. With the development of micro-nanofabrication technology, the characteristic size of the grating becomes smaller and the subwavelength grating (SWG) waveguide has attracted much attention in recent years. In the SWG waveguide, the grating period is much smaller than the wavelength of light propagating in it [21]. Furthermore, the dispersion relation of the mode in the SWG waveguide can be changed by adjusting its period and duty cycle [22]. These excellent properties have led to the innovation of many SWG-based devices [23], such as MMI couplers [24], polarization-independent DCs [25], subwavelength waveguide crossings [26], etc. In addition, the SWG waveguide is also employed for polarization management devices, including the polarization rotator [27,28] and PBS [29–31]. However, in the conventional two-waveguide DC structure, a taper region is always required to transform the SWG waveguide to the conventional waveguide, which can complicate the fabrication process and increase the overall device length.

In this paper, we propose an ultracompact PBS by using a triple-waveguide DC (TWDC) structure which is formed by

two silicon waveguides and a SWG waveguide sandwiching between them. By properly adjusting the structural parameters of the SWG, only the injected TE mode is efficiently coupled between the silicon waveguides and SWG waveguide, while the TM mode is unaffected. Due to the extremely high coupling efficiency within a short distance, the TWDC-based PBS offers a compact size with a coupling length of 6.5 μm. Furthermore, the ER and insertion loss (IL) for both the TE mode and TM mode are higher than 27 dB and lower than 0.3 dB at a wavelength of 1550 nm, respectively.

2. DESIGN PRINCIPLE

Figure 1 shows the cross section and 3D schematics of the proposed PBS. The device is based on the silicon-on-insulator platform with a top silicon thickness of 340 nm. We use a dual-coupling scheme between the silicon waveguides and the SWG waveguide so that no taper is needed to transfer the SWG mode to the silicon waveguide mode. The width of the two silicon waveguides is equal ($w_1 = w_3 = 250$ nm). The SWG waveguide is composed of Si and SiO_2 (with refractive indices of 3.476 and 1.444 at 1550 nm, respectively), wherein the duty cycle of Si is a/Λ, and Λ is the period of the SWG waveguide, which is set to 300 nm to effectively suppress the diffraction effect and ensure that the grating is effectively applied in the subwavelength region.

The material equivalent refractive index n_B of the SWG waveguide can be estimated according to Rytov's formula [32]:

$$n_B^2 \approx \frac{a}{\Lambda} n_{\mathrm{GH}}^2 + \frac{\Lambda - a}{\Lambda} n_{\mathrm{GL}}^2, \tag{1}$$

where n_{GH} and n_{GL} are the high and low refractive indices in the SWG, respectively. According to Eq. (1), n_B decreases as the duty cycle becomes lower, and the effective mode indices n_{eff} in the SWG waveguide also necessarily exhibit a decreasing relationship with a/Λ.

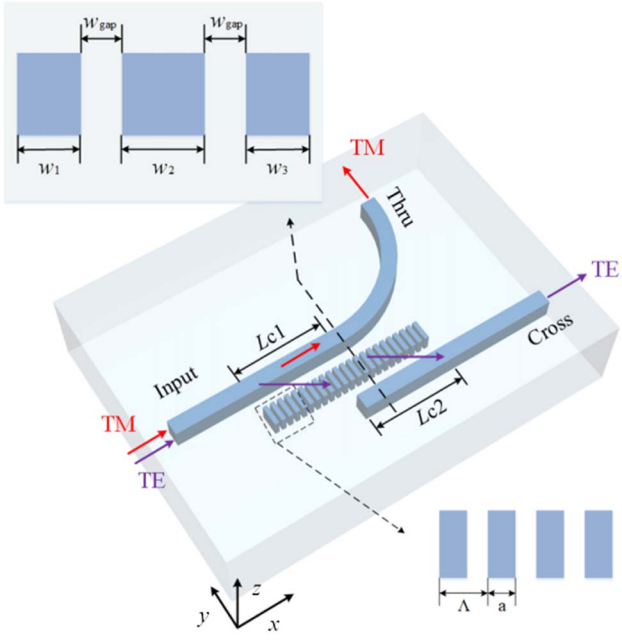

Fig. 1. Schematics of the proposed PBS.

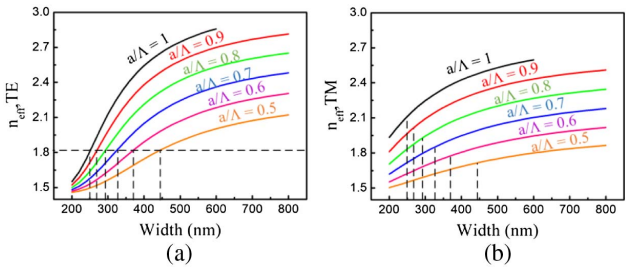

Fig. 2. Effective indices variation of the (a) TE mode and (b) TM mode with different duty cycles. The transverse dashed line represents the effective refractive index for phase matching of the TE mode, and the vertical dashed line corresponds to the width of different waveguides under this matching condition.

The effective refractive indices of the TE and TM modes in the SWG waveguide with different duty cycles ($a/\Lambda = 0.5$–0.9) and conventional silicon waveguides ($a/\Lambda = 1$) are shown in Fig. 2. It can be seen that the TE mode can be easily phase matched to the SWG waveguide with various duty cycles. While there is an effective index gap between the silicon waveguide and the SWG waveguide when the duty cycle is smaller than 0.6. Therefore, the TM mode is more difficult to couple from the silicon waveguide to the SWG waveguide. Bearing this in mind, we set the width of the traditional silicon waveguide to 250 nm, corresponding to $n_{\mathrm{eff,TE}} = 1.809$ and $n_{\mathrm{eff,TM}} = 2.113$. To satisfy the phase-matching condition, the widths of the SWG are approximately 265 nm, 290 nm, 320 nm, 365 nm, and 435 nm for a/Λ from 0.9 to 0.5, respectively.

Since the effective refractive index obtained by Eq. (1) is only an approximation value, in order to get more accurate structure parameters, we use the 3D finite-difference time-domain method to simulate the coupling between the two waveguides. In the simulation, we use a SiO_2 substrate with a finite thickness of 2 μm to avoid leakage loss [33]. By using the theoretical SWG width w_2 as the basis and changing the value slightly, the coupling efficiency dependence on w_2 is shown in Fig. 3. It is found that SWG waveguides with duty cycles of 0.7, 0.6, and 0.5 have optimized widths of 370 nm, 420 nm, and 490 nm, respectively, which is about 50 nm wider compared with the ones obtained by the equivalent refractive index

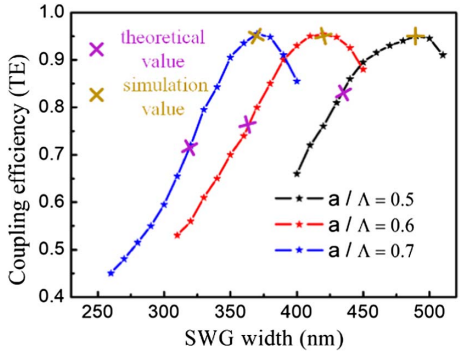

Fig. 3. Influence of SWG waveguide width on coupling efficiency of the TE mode under different duty cycles.

method. In order to make a more accurate initial parameters approximation, calculating the Floquet–Bloch mode of a 2D periodic grating can be implemented to replace the Rytov's method [34]. In our design, in order to guide the TE mode toward the cross port, the SWG width w_2 with a duty cycle of 0.6 is chosen to be 420 nm. In fact, for other duty cycles, it is flexible to select the appropriate width according to the results shown in Fig. 3. Therefore, the SWG structure offers more design freedom.

An appropriate gap is essential for efficient coupling. Taking into account the 248 nm optical lithography technology [35], the gap size w_{gap} is fixed to be 200 nm in the design. And the coupling region is composed of two coupling regions with $Lc1$ and $Lc2$. According to the supermode theory, L_c can be calculated as follows [36]:

$$L_c = \frac{\lambda_0}{2(n_{even} - n_{odd})}, \tag{2}$$

where $\lambda_0 = 1.55$ μm is the free-space wavelength, and n_{even} and n_{odd} are the effective refractive indices for even and odd supermodes, respectively. Under $w_{gap} = 200$ nm, the calculated L_c is 3.88 μm. Furthermore, a 90° bend with a radius of 3 μm is installed in the PBS to decouple the TE mode from the SWG waveguide. According to our calculation, such a radius is sufficient to avoid prominent loss.

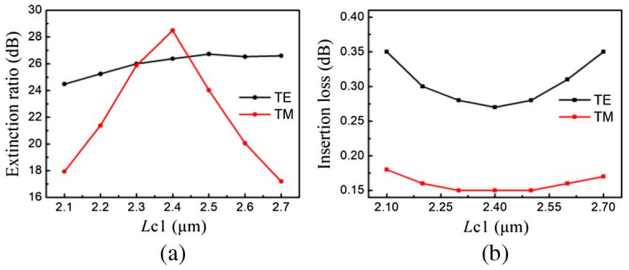

Fig. 4. Influence of $Lc1$ on (a) ER and (b) IL, respectively.

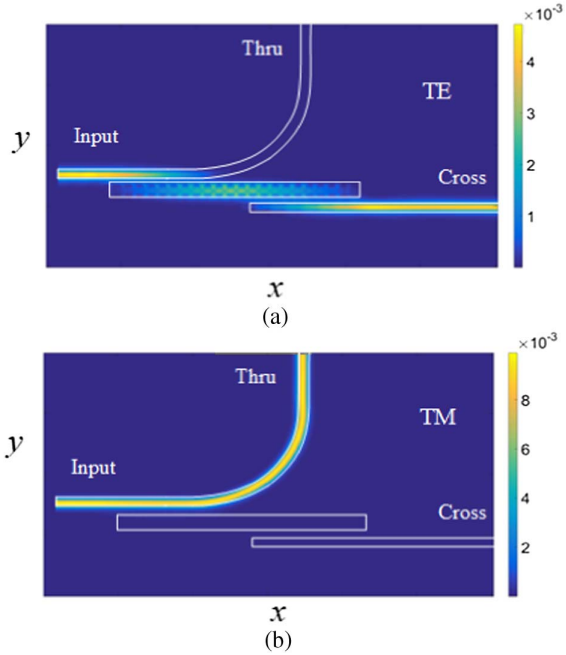

Fig. 5. Power distributions in PBS with TE (a) and TM (b) light injection.

3. RESULTS AND DISCUSSION

The performance of the PBS is evaluated by ER and IL. The impact of $Lc1$ on the PBS performance is summarized in Fig. 4. Since the coupling occurs for the TE mode, it can be seen that the PBS performances (ER of the TM mode and IL of the TE mode) have relatively strong dependence on the change of $Lc1$. The results show that the optimized $Lc1$ is 2.4 μm, which is slightly shorter than the one obtained by supermode theory. In fact, according to the device structure in Fig. 1, in the first coupling region, light in the front part of the bend waveguide and the SWG waveguide will still interact with each other because of the gradual distance change between them, which may result

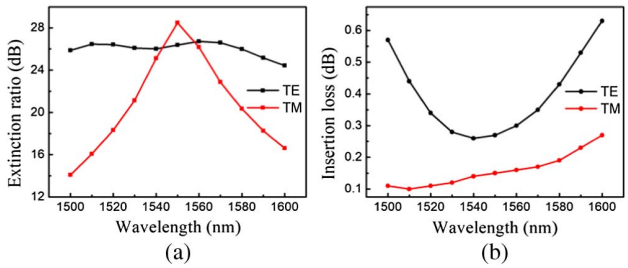

Fig. 6. (a) ER and (b) IL in the TE mode and TM mode at different wavelengths.

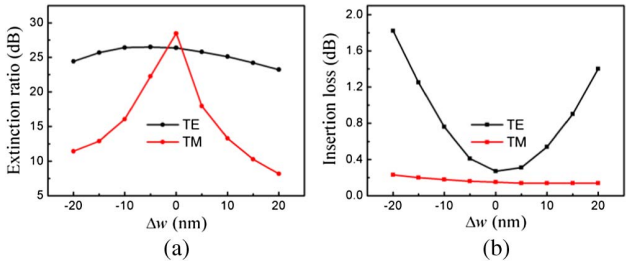

Fig. 7. Dependence of the (a) ER and (b) IL in the TE mode and TM mode on the width variation.

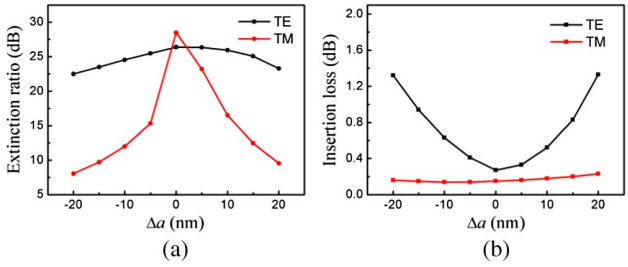

Fig. 8. Dependence of the (a) ER and (b) IL in the TE mode and TM mode on the duty cycle variation.

Table 1. Comparison of Several PBSs

Reference	Platform	Fab.	Length	Max. IL at Bandwidth	Min. ER at Bandwidth	Tolerance for Width
[29]	$H = 340$ nm MFS[a] = 100 nm	No	21 μm	1.5 dB at 115 nm	10 dB at 115 nm	$\Delta w = -30$ nm for ER > 10 dB
[30]	$H = 250$ nm MFS[a] = 100 nm	No	6.8 μm	0.71 dB at 115 nm	18 dB at 81 nm	$\Delta w = -50$ nm for ER > 18 dB
[31]	$H = 220$ nm MFS[a] = 150 nm	Yes	23 μm	1 dB at 60 nm	20 dB at 60 nm	NA[b]
Our work	$H = 340$ nm MFS[a] = 120 nm	No	6.5 μm	0.63 dB at 100 nm	20 dB at 60 nm	$\Delta w = -10$ nm for ER > 15 dB

[a]MFS: minimum feature size.
[b]NA: not available.

in power recoupling. To avoid such excessive coupling, it is necessary to shorten the length of $Lc1$. Combining with the previous theoretical calculation by Eq. (2) for $Lc2$ (∼3.9 μm), the length of the SWG waveguide (coupling region) is determined to be 6.5 μm.

Figure 5 is the results of the power transmission performance in the PBS at a wavelength of 1550 nm with $w_1 = w_3 = 250$ nm, $w_2 = 420$ nm, $w_{gap} = 200$ nn, $Lc1 + Lc2 = 6.5$ μm, $a/\Lambda = 0.6$, and $\Lambda = 300$ nm. As predicted, the TE and TM modes are perfectly separated with negligible loss. Due to the modified dispersion relation induced by the SWG waveguide, it acts as a bridge for the TE mode while brings little perturbation for the TM mode. Benefiting from the refractive index controllability of SWG waveguides, no other lossy media such as metal [17–19] is used in the PBS, so the two modes maintain extremely high efficiency output on the thru and cross ports.

Figure 6 shows the relation between the ER and IL of the PBS with the change of wavelength. At a wavelength of 1550 nm, the ERs of the TE mode and TM mode reach 26.4 dB and 28.5 dB, respectively. Since the TE mode experiences coupling for two times, the IL of the TE mode is slightly higher than that of the TM mode. Nevertheless, 0.3 and 0.2 dB are still excellent. The bandwidth for ER > 20 dB is about 60 nm, covering the entire C-band, and the bandwidth for ER > 10 dB achieves 100 nm. Within the wavelength simulation range of 1500–1600 nm, the ILs of the two modes are lower than 0.6 dB and 0.3 dB, respectively.

Next, we investigate the manufacturing tolerance of the designed PBS for width w and duty cycle a; the results are shown in Figs. 7 and 8. Δw means the width of the three waveguides of the PBS varies simultaneously, with positive values corresponding to wider width and negative values corresponding to narrower width. Since the difference of the TM mode between two waveguides is relatively large, it is insensitive to structural changes, which leads to the fact that the ER of the TE mode and the IL of the TM mode are in a stable state, while the ER of the TE mode and IL of the TM mode are more sensitive. Considering that electron beam lithography (EBL) usually guarantees a resolution of 10 nm [14], when Δw or Δa change ±10 nm, the ERs of the TE and TM modes are >20 dB and >10 dB, and the ILs of the two modes are <0.8 dB and <0.2 dB, respectively.

Table 1 summarizes several previous results of the SWG-based PBSs. Comparing with them, it can be seen that our PBS has the advantages of the short length and low loss. The width tolerance is sensitive but still within the capability of EBL technology.

4. CONCLUSION

We have proposed and investigated an ultracompact and high-performance PBS with the assistance of a TWDC consisting of two silicon waveguides and a SWG waveguide. Tailoring the SWG waveguide by changing the duty cycle and other factors can make two orthogonal polarizations have different transmission performances. The TE mode experiences two efficient coupling processes within only 6.5 μm length, allowing a compact device footprint. With the optimized structure, the PBS offers high ER and low IL of 26.38 dB (28.48 dB) and 0.27 dB (0.15 dB) for TE (TM) at the wavelength of 1550 nm, respectively. Without a tapering region and metal structure, the device is simple and can be easily realized by mature manufacturing technology. The device has potential application prospects in the compact integrated optical circuits.

Funding. Hubei Key Laboratory of Inland Shipping Technology (NHHY2018002); National Natural Science Foundation of China (NSFC) (61605179); Wuhan Municipal Science and Technology Bureau (2018010401011297); Experimental Technology Research Funds (SJ-201816); China University of Geosciences, Wuhan (CUG) (162301132703, CUG2018JM16, G1323511794).

REFERENCES

1. T. Barwicz, M. R. Watts, M. A. Popovic, P. T. Rakich, L. Socci, F. X. Kartner, E. P. Ippen, and H. I. Smith, "Polarization-transparent microphotonic devices in the strong confinement limit," Nat. Photonics **1**, 57–60 (2007).
2. D. Dai, L. Liu, S. Gao, D. X. Xu, and S. He, "Polarization management for silicon photonic integrated circuits," Laser Photonics Rev. **7**, 303–328 (2013).
3. D. Dai, Z. Wang, J. Peters, and J. E. Bowers, "Compact polarization beam splitter using an asymmetrical Mach-Zehnder interferometer based on silicon-on-insulator waveguides," IEEE Photonics Technol. Lett. **24**, 673–675 (2012).
4. J. Li, H. Liu, and L. Zhang, "Terahertz wave polarization beam splitter using a cascaded multimode interference structure," Appl. Opt. **53**, 5024–5028 (2014).
5. X. Sun, M. Z. Alam, J. S. Aitchison, and M. Mojahedi, "Compact and broadband polarization beam splitter based on a silicon nitride augmented low-index guiding structure," Opt. Lett. **41**, 163–166 (2016).

6. D. Dai, Z. Wang, and J. E. Bowers, "Ultrashort broadband polarization beam splitter based on an asymmetrical directional coupler," Opt. Lett. **36**, 2590–2592 (2011).
7. D. W. Kim, M. H. Lee, Y. Kim, and K. H. Kim, "Planar-type polarization beam splitter based on a bridged silicon waveguide coupler," Opt. Express **23**, 998–1004 (2015).
8. C. Hsu, T. Chang, J. Chen, and Y. Cheng, "8.13 μm in length and CMOS compatible polarization beam splitter based on an asymmetrical directional coupler," Appl. Opt. **55**, 3313–3318 (2016).
9. L. Chang, L. Liu, Y. Gong, M. Tan, Y. Yu, and Z. Li, "Polarization-independent directional coupler and polarization beam splitter based on asymmetric cross-slot waveguides," Appl. Opt. **57**, 678–683 (2018).
10. Y. Xu and J. Xiao, "Design of a compact and integrated TM-rotated/TE-through polarization beam splitter for silicon-based slot waveguides," Appl. Opt. **55**, 611–618 (2016).
11. N. Saidani, W. Belhadj, F. AbdelMalek, and H. Bouchriha, "Detailed investigation of self-imaging in multimode photonic crystal waveguides for applications in power and polarization beam splitters," Opt. Commun. **285**, 3487–3492 (2012).
12. G. Mo and J. Li, "Compact terahertz wave polarization beam splitter using photonic crystal," Appl. Opt. **55**, 7093–7097 (2016).
13. Y. Kim, M. H. Lee, Y. Kim, and K. H. Kim, "High-extinction-ratio directional-coupler-type polarization beam splitter with a bridged silicon wire waveguide," Opt. Lett. **43**, 3241–3244 (2018).
14. J. Feng, R. Akimoto, and H. Zeng, "Asymmetric silicon slot-waveguide-assisted polarizing beam splitter," IEEE Photonics Technol. Lett. **28**, 1294–1297 (2016).
15. J. R. Ong, T. Y. L. Ang, E. Sahin, B. Pawlina, G. F. R. Chen, D. T. H. Tan, S. T. Lim, and C. E. Png, "Broadband silicon polarization beam splitter with a high extinction ratio using a triple-bent-waveguide directional coupler," Opt. Lett. **42**, 4450–4453 (2017).
16. F. Zhang, H. Yun, Y. Wang, Z. Lu, L. Chrostowski, and N. A. F. Jaeger, "Compact broadband polarization beam splitter using a symmetric directional coupler with sinusoidal bends," Opt. Lett. **42**, 235–238 (2017).
17. X. Guan, H. Wu, Y. Shi, L. Wosinski, and D. Dai, "Ultracompact and broadband polarization beam splitter utilizing the evanescent coupling between a hybrid plasmonic waveguide and a silicon nanowire," Opt. Lett. **38**, 3005–3008 (2013).
18. J. Chee, S. Zhu, and G. Q. Lo, "CMOS compatible polarization splitter using hybrid plasmonic waveguide," Opt. Express **20**, 25345–25355 (2012).
19. B. Ni and J. Xiao, "Ultracompact and broadband silicon-based polarization beam splitter using an asymmetrical directional coupler," IEEE J. Quantum Electron. **53**, 8400208 (2017).
20. J. Xiao and Z. Guo, "Ultracompact polarization-insensitive power splitter using subwavelength gratings," IEEE Photonics Technol. Lett. **30**, 529–532 (2018).
21. P. J. Bock, P. Cheben, J. H. Schmid, J. Lapointe, A. Delâge, S. Janz, and T. J. Hall, "Subwavelength grating periodic structures in silicon-on-insulator: a new type of microphotonic waveguide," Opt. Express **18**, 20251–20262 (2010).
22. R. Halir, P. J. Bock, P. Cheben, A. Ortega-Moñux, C. Alonso-Ramos, J. H. Schmid, J. Lapointe, D. Xu, J. G. Wangüemert-Pérez, I. Molina-Fernandez, and S. Janz, "Waveguide sub-wavelength structures: a review of principles and applications," Laser Photonics Rev. **9**, 25–49 (2015).
23. R. Halir, A. Ortega-Moñux, D. Benedikovic, G. Z. Mashanovich, J. G. Wangüemert-Pérez, J. H. Schmid, I. Molina-Fernandez, and P. Cheben, "Subwavelength-grating metamaterial structures for silicon photonic devices," Proc. IEEE **106**, 2144–2157 (2018).
24. A. Maese-Novo, R. Halir, S. Romero-Garcıa, D. Perez-Galacho, L. Zavargo-Peche, A. Ortega-Monux, I. Molina-Fernandez, J. G. Wanguemert-Perez, and P. Cheben, "Wavelength independent multimode interference coupler," Opt. Express **21**, 7033–7040 (2013).
25. Y. Wang, X. Wang, J. Flueckiger, H. Yun, W. Shi, R. Bojko, N. A. F. Jaeger, and L. Chrostowski, "Focusing sub-wavelength grating couplers with low back reflections for rapid prototyping of silicon photonic circuits," Opt. Express **22**, 20652–20662 (2014).
26. P. P. J. Bock, P. Cheben, J. H. Schmid, J. Lapointe, A. Delâge, D. X. Xu, S. Janz, A. Densmore, and T. J. Hall, "Subwavelength grating crossings for silicon wire waveguides," Opt. Express **18**, 16146–16155 (2010).
27. S. Wu and J. Xiao, "Compact polarization rotator for silicon-based cross-slot waveguides using subwavelength gratings," Appl. Opt. **56**, 4892–4899 (2017).
28. Y. Xiong, J. G. Wangüemert-Pérez, D. Xu, J. H. Schmid, P. Cheben, and W. N. Ye, "Polarization splitter and rotator with subwavelength grating for enhanced fabrication tolerance," Opt. Lett. **39**, 6931–6934 (2014).
29. L. Liu, Q. Deng, and Z. Zhou, "Manipulation of beat length and wavelength dependence of a polarization beam splitter using a subwavelength grating," Opt. Lett. **41**, 5126–5129 (2016).
30. Y. Xu and J. Xiao, "Compact and high extinction ratio polarization beam splitter using subwavelength grating couplers," Opt. Lett. **41**, 773–776 (2016).
31. S. Chen, H. Wu, and D. Dai, "High extinction-ratio compact polarisation beam splitter on silicon," Electron. Lett. **52**, 1043–1045 (2016).
32. S. M. Rytov, "Electromagnetic properties of a finely stratified medium," J. Exp. Theor. Phys. **2**, 466–475 (1956).
33. J. D. Sarmiento-Merenguel, A. Ortega-Moñux, J. M. Fédéli, J. G. Wangüemert-Pérez, C. Alonso-Ramos, E. Duran-Valdeiglesias, P. Cheben, I. Molina-Fernandez, and R. Halir, "Controlling leakage losses in subwavelength grating silicon metamaterial waveguides," Opt. Lett. **41**, 3443–3446 (2016).
34. J. D. Joannopoulos, S. G. Johnson, J. N. Winn, and R. D. Meade, "Symmetries and solid-state electromagnetism," in *Photonic Crystals*, 2nd ed. (Princeton University, 2008), pp. 25–43.
35. Y. Huang, J. Song, X. Luo, T. Y. Liow, and G. Q. Lo, "CMOS compatible monolithic multi-layer SiN_4 on SOI platform for low-loss high performance silicon photonics dense integration," Opt. Express **22**, 21859–21865 (2014).
36. J. Donnelly, "Limitations on power-transfer efficiency in three-guide optical couplers," IEEE J. Quantum Electron. **22**, 610–616 (1986).